Electron Orbits in Solar Reconnecting Current Sheets

C. Gontikakis*, C. Efthymiopoulos* and A. Anastasiadis†

* *Academy of Athens, Research Center of Astronomy and Applied Mathematics, Soranou Efessiou 4, GR-11527 Athens Greece.*
† *National Observatory of Athens, Institute for Space Applications and Remote sensing 15236 Penteli Greece*

Abstract. We investigate the orbits of charged particles (electrons) that interact with a 3D-solar type reconnecting current sheet (RCS). The magnetic field used is a linearized Harris type model. Particles are accelerated by a super-Dreicer electric field. Taking advantage of the translational symmetries of the fields, the orbits computation is simplified to integration of the equations of motion in a Hamiltonian of two degrees of freedom. The application of canonical transformations, constructed with Lie series, transforms the Hamiltonian to a normal form. The conditions for which electrons are trapped in the RCS are derived analytically. For escaping particles, the amount of final kinetic energy gain or loss is described with analytical expressions that are in good agreement with the numerical results.

Keywords: Solar flares; non-linear dynamics; particles acceleration; Chaotic motion
PACS: 95.10.Fh;96.60.ql;96.50.Pw

INTRODUCTION

Charged particle's acceleration occurs in various space environments. One case of particular interest is the eruption of solar flares. Evidence that particle acceleration takes place during these events is given by the spectrum of hard X-rays, produced by *supra thermal* electron distributions. Such distributions include more high energy electrons than expected by a Maxwellian distribution of 10^7 K, which is the temperature of solar flares plasma [19].

The mechanism that accelerates particles should involve reconnecting current sheets (RCS). A RCS is a magnetic discontinuty where oppositely oriented magnetic fields come close in very small length scales. Current sheets are formed spontaneously in the solar magnetic field [16] in sites of magnetic reconnection [17]. Most magnetic reconnection topologies involve strong electric fields that are crucial to the effect of particle acceleration.

The study of particles motion in such magnetic topologies started soon after the discovery of the Earth magnetotail current sheet, which is responsible for the particle precipitation in the Earth atmosphere during substorms [17]. As the magnetic field reversal takes place in length scales comparable to the Larmor radius, one has to solve the equations of motion in detail in order to study the particle orbits. In the work of [18] a familly of orbits is found based on an analytical study. Several studies have been performed, based on detailed analysis of particles interacting with the Earth Magnetotail (see [3] for a review).

CP848, *Recent Advances in Astronomy and Astrophysics,*
7th International Conference of the Hellenic Astronomical Society, edited by N. H. Solomos

In the case of solar flares, the same formalism can be applied despite the difference in the values of magnetic and electric fields, which are much larger in the solar atmosphere than in the Earth magnetotail. In the solar plasma, particle acceleration can also be treated as a collisionless process when strong electric fields are present. This is because the electric field accelerates the particles to large velocities compared to the mean thermal velocity ([1], [14]).

One the other hand, measurements at the level of the photosphere using vector magnetographs [8] have shown that, during the first phase of flares, the magnetic field is strongly sheared. This suggests the importance of a *longitudinal* magnetic component, parallel to the electric field. As in the case of the Earth magnetotail, the perpendicular magnetic component introduces a perturbation to the particle's motions [18]. Particle acceleration in a RCS with non zero shear was investigated in [10], [11], [12]. In these papers, scaling formulas are derived for the final kinetic energy gain of particles as a function of the values of the various components of the magnetic field. In [5] and [6], we studied the behavior of particle orbits by dynamical systems' methods.

In the following section, numerical simulations are presented in order to show some characteristics of the electron motion in RCSs. This includes examples of electrons trapped inside current sheets or of escaping electrons gaining or losing kinetic energy. Poincaré sections are used to show the nature of the orbits inside the RCS. A detailed analysis of these phenomena is given elsewhere ([5],[6]).

THE MODEL

The topology of the magnetic and electric fields is given by Eqs (1). The B_x component represents a first order truncation of the Harris-type configuration, as the variation across the current sheet is linear. The components along the y and z axes are constant. The component along the z axis is called longitudinal component and represents the shear of the magnetic field.

$$\begin{aligned} E &= (0,0,E), \quad B = (-y, \xi_\perp, \xi_\parallel) B_0 \qquad \text{for } |y| \leq 1 \\ E &= (0,0,0), \quad B = (-y/|y|, \xi_\perp, \xi_\parallel) B_0 \quad \text{for } |y| > 1 \end{aligned} \tag{1}$$

The RCS extents up to $|y| = 1$. Beyond this limit, the magnetic field is considered constant. In our numerical simulations we consider that when a particle reaches this limit it escapes from the current sheet. The equations of motion of a charged particle moving in these fields are given by

$$\frac{d^2x}{dt^2} = \xi_\parallel \frac{dy}{dt} - \xi_\perp \frac{dz}{dt} \tag{2}$$

$$\frac{d^2y}{dt^2} = -\xi_\parallel \frac{dx}{dt} - y\frac{dz}{dt} \tag{3}$$

$$\frac{d^2z}{dt^2} = \varepsilon + \xi_\perp \frac{dx}{dt} + y\frac{dy}{dt} \tag{4}$$

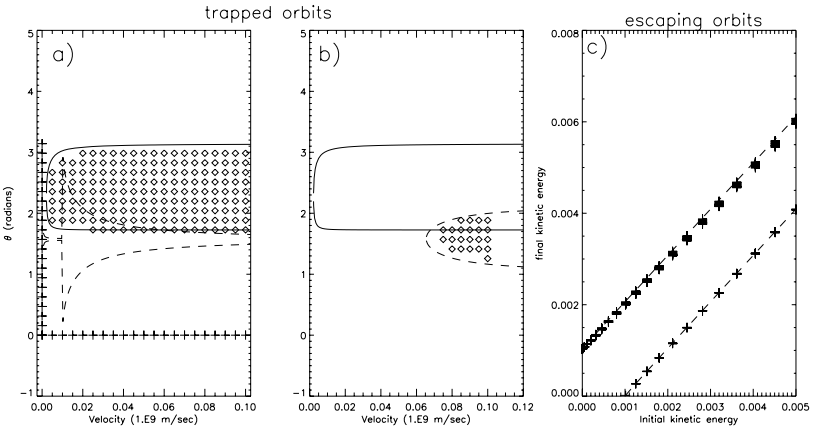

FIGURE 1. Initial conditions of trapped orbits in an RCS with $\xi_\perp = 10^{-2}, \varepsilon = 10^{-5}$ and $\xi_\parallel = 0$ (no-shear). Diamonds correspond to the initial conditions of injection (υ, θ) (see text) for which a particle remains trapped in the current sheet. The solid curve represents an analytical approximation of the trapping domain developed in [6], which is valid in the no-shear limit ($\xi_\parallel \to 0$). The dashed curve represents a different analytical approximation of the trapping domains based on a low order adiabatic invariant [5] [6], which is not succesful. b) Same as a) when the shear is strong ($\xi_\parallel = 1$). The second analytical approximation is now succesful. c) Final kinetic energy of escaping particles against their initial kinetic energy. The RCS parameters are as in (a). The energy unit is 1.9×10^3 keV.

Equations 2,3,4 are written for a positive charge and are scaled to dimensionless units so that the electric field is given by $\varepsilon = mE/(qB_0^2)$ whereas the unit of time is the inverse of the Larmor frequency $t = \omega^{-1} = m/(qB_0)$. In this study the magnetic field is $B_0 = 100$ G and the electric field $E = 100$ V/m, which corresponds to $\varepsilon = 10^{-5}$. These are typical values for the fields measured in solar flares (see [14]). Furthermore, except of the total energy E, a second constant of motion $I_2 = \dot{x} - \xi_\parallel y + \xi_\perp z$, can be derived by integrating Eq. 2. Using I_2 one can derive a Hamiltonian of two degrees of freedom to describe the particles motion instead of three as in Eqs. (2,3,4).

$$H = \frac{1}{2}p_y^2 + \frac{1}{2}(c_4 + \frac{1}{2}y^2)^2 + \frac{1}{2}(I_2 - \xi_\perp z + \xi_\parallel y)^2 - \varepsilon z \tag{5}$$

where $c_4 = \xi_\perp x + p_z$. The new canonically conjugate pairs are (y, p_y) and (z, c_4), where: $p_y = \dot{y}$ and $p_z = \dot{z} - (\xi_\perp x + 0.5y^2)$. The canonical momentum p_z is the sum of the velocity and the magnetic vector potential component (see [5], [6]). Integrating the Hamiltonian equations using he function $H(y, z, p_y, c_4)$ described by Eq. 5, we performed numerical simulations presented in the following section.

NUMERICAL SIMULATIONS

Trapped and escaping particles

We investigated two examples of RCS models with zero shear ($\xi_{\parallel} = 0$) or strong shear ($\xi_{\parallel} = 1$). In our scaled units, the electric field is $\varepsilon = 10^{-5}$ and the perpendicular component $\xi_{\perp} = 10^{-2}$. Particles are initially injected at the center of the current sheet (y=z=0). The initial velocity orientation is chosen in a range from $\theta = 0$ to π where θ is the angle of the velocity with the z axis. The dimensionless velocity range is 0 - 0.1, corresponding to 0-10^8 m/sec. For several orbits starting with these initial conditions, particles remain trapped into the sheet ($|y| < 1$) or eventually escape from it. The computation of the final kinetic energy provides a measure of the effectiveness of the RCS as an accelerator.

In Figure 1, the axes refer to a particle's initial velocity (orientation θ, and magnitude v_0). Each diamond corresponds to a particle that remained trapped in the sheet until the end of the numerical integration. In the case of non-shear (Fig 1a) we notice that orbits are trapped for any value of v_0 as long as $1.7 < \theta < \pi$. In the case of large shear, (Fig 1b), the trapped domain shrinks considerably so that for $v_0 < 0.07$ particles always escape from the sheet.

The domain of trapped orbits, defined in the (v_0, θ) plane can be described by analytical approximations. This was done in two limits: 1) $\xi_{\parallel} \to 0$ and 2) $\xi_{\parallel} \to 1$ (see [5], [6]). Both theoretical limits are represented in Fig. 1, the first with a solid curve and the second with a dashed curve. Each approximation is succesfull in the case where the corresponding limit holds (case 1 for Fig 1a and case 2 for Fig 1b respectively).

In Fig. 1c, the kinetic energy gain of particles escaping the RCS with strong shear is plotted against their initial kinetic energy. Two groups of particles are distinguished: particles gainning or losing kinetic energy. The maximum kinetic energy gain of a particle can be described with good accuracy from our analytic model (see [5], [6]) shown as the dashed lines in Fig 1c. In particular, for particles escaping along chaotic orbits, the minimum and maximum acceleration lengths are provided by the zero velocity curves, found from Eq. (5) by setting $\dot{y} = \dot{z} = 0$:

$$\xi_{\parallel}^2 y^2 + \xi_{\perp}^2 z^2 - 2\xi_{\parallel}\xi_{\perp} yz - 2\varepsilon z = 2E \tag{6}$$

When $\xi_{\parallel} \neq 0$ Eq. (6) is a parabola open in the half plane $y > 0$. For $y = 1$, Eq. (6) yields two solutions: $z = z_{min}$ or $z = z_{max}$. A particle leaving the sheet from z_{max} has the maximum possible kinetic energy gain. If the particle initial kinetic energy is strong enough, the particle can leave the current sheet from $y = -1$. In this case the particle loses kinetic energy (particles in Fig 1c below the diagonal).

Poincaré sections

A useful diagnostic tool for studying orbits is to compute Poincaré sections. In the present study, Poincaré sections are computed by tracing the crossing orbits on the $(\dot{z}, z)$

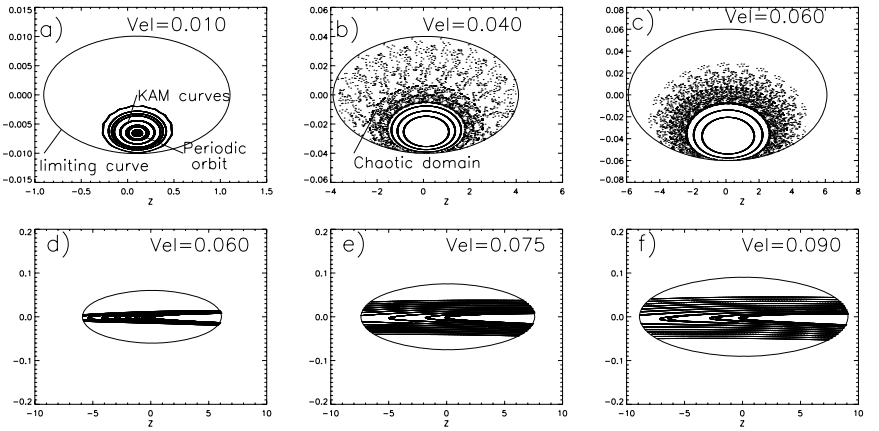

FIGURE 2. Poincaré sections $(\dot{z}, z)$ for several initial kinetic energies of particles. The first row of panels is computed using $\xi_\perp = 10^{-2}, \xi_\parallel = 0, \varepsilon = 10^{-5}$ (as panel a of Fig 1). In the second row $\xi_\perp = 10^{-2}, \xi_\parallel = 1, \varepsilon = 10^{-5}$. The initial particle velocity is indicated in each panel.

plane when $y = 0, \dot{y} > 0$. Fig. 2 shows several examples of Poincaré sections computed for orbits with different initial energies for the same model parameters as in the two examples of Fig 1.

On the Poincaré section, orbits cannot give intersections outside a limiting curve. The limiting curve, from Eq. (5), is $\dot{z}^2 + \xi_\perp^2 (z - \varepsilon/\xi_\perp^2)^2 = 2E + (\varepsilon/\xi_\perp)^2$ where E is the energy of the particle. One of the trapped orbits is periodic and intersects the Poincaré section at a single point. Most other trapped orbits intersect the Poincaré section in a way forming KAM curves ([13],[2], [15]) which are either closed, around the periodic orbit (Figs 2a,b,c) or elliptic arcs that intersect the limiting curve (Figs 2d,e,f). The KAM curves determine the region of non-chaotic motion where particles follow either periodic or quasi-periodic orbits. Between the last KAM curve and the limiting curve lies a large chaotic region. Chaotic orbits explore all the available phase space between the last KAM torus and the zero velocity surface. The KAM curves cross the $z = 0$ axis in Fig 2, so that trapped orbits of Fig 1 starting at $y = z = 0$ correspond to KAM curves. In the case of no shear (Figs. 2a,b,c) the Poincaré section shows a region of regular motion organized around periodic orbits, surrounded by a chaotic domain. In this case, only chaotic particles escape from the sheet. The last KAM curve, which separates the two domains, is tangent to the limiting curve. As we increase the initial particle velocity, the area included in the limiting curve increases. For strong magnetic shear, (Figs. 2d,e,f) the morphology is very different. KAM curves cover all the available area, and they form elongated elliptic arcs that intersect the limiting curve. This results in that particles can escape form the sheet along regular orbits, when the corresponding KAM torus intersects the planes $y \pm 1$.

THEORETICAL ANALYSIS

The existence of regular orbits forming KAM curves on the Poincaré surfaces is a manifastation of the existence of a third constant of motion (named J_1') besides E, I_2. J_1' is preserved along regular orbits but not along chaotic orbits. J_1' corresponds to an adiabatic invariant of the particle bouncing inside the magnetic trap (see [9] Chapter 2.3). In [5] J_1' is computed as a series in the parameters $\xi_\perp, \xi_\parallel, \varepsilon$. The initial Hamiltonian is transformed into a normal form using Lie series. For $\xi_\parallel = 1$, the expression for J_1' is simplified and one can compute the KAM curves as well as the shape of the trapping domain for (see [5], [6]).

For $\xi_\parallel = 0$, the last KAM is an ellipse which is almost tangent to the limiting curve (see Figs. 2a,b,c). The shape of KAM as well as the position of the periodic orbit on the Poincaré sections, are obtained [6] using the averaging technique known in celestrial mechanics as 'Hadjidimitriou mapping' [7].

CONCLUSIONS

In this work the motion of electrons inside a RCS is analysed. Two types of RCS are studied, with zero or strong magnetic shear.

Numerical simulations show that, in both cases, electrons for particular initial conditions can be trapped in the RCS. The trapping domain is more extended in the case of zero shear.

With the help of Poincaré sections, we find that in the case of strong shear, both trapped and escaping electrons mostly follow regular orbits. On the other hand, in the case of zero shear electrons escape from the sheet following chaotic orbits while most regular orbits are trapped.

Regular orbits can be analysed by calculating a third integral of motion. This integral is calculated by the method of Lie-series (see [5] for the mathematical details.)

Trapped particles must be important for the self-consistency of solar RCS, (see [4] section 5.4). They could also affect the total number of accelerated particles during solar flares.

ACKNOWLEDGMENTS

This work was supported by the Research Committee of the Academy of Athens.

REFERENCES

1. A. Anastasiadis, C. Gontikakis, N. Vilmer and L. Vlahos, *Astron. & Astroph.*, **422** 323–330, (2004).
2. V. I. Arnold, *Russ. Math. Surv.*, 18 (5), 9; (6), 91 1963
3. J. Chen, *J. Geophys. Res.*, **97**, 15011–15050, (1992).
4. S. W. H. Cowley, *Solar Systems Magnetic Fields, Geophysics and Astrophysics Monographs*, Ed. E. Priest, Reidel Publishing Company, 121–155 (1985).
5. C. Efthymiopoulos, C. Gontikakis, and A. Anastasiadis, *Astron. & Astroph.*, **443** 663–678, (2005).

6. C. Gontikakis, C. Efthymiopoulos, and A. Anastasiadis, *M.N.R.A.S.*, in press (2006).
7. J.D. Hadjidemetriou, *Predictability, Stability and Chaos in N-Body Dynamical Systems*, Ed. A.E. Roy, Plenum Press, New York, 157-175 (1991).
8. M. J. Hagyard *Mem. S.A. It.* **61**, 337. (1990).
9. A. J. Lichtenberg, and M. A. Lieberman *Regular and Chaotic Dynamics*, Springer Verlag, New York, (1991).
10. Y. E Litvinenko, *Sol. Phys.*, **147**, 337. (1993).
11. Y. E. Litvinenko, and B. V. Somov, *Sol. Phys.*, **146**, 127 (1993).
12. Y. E. Litvinenko, *Astrophys. J.*, **462**, 997 (1996).
13. A. N. Kolmogorov, *Dokl. Akad. Nauk. SSSR* **119**, 527 (1954).
14. P. C. H. Martens and A. Young *Astrophys. J. Suppl.*, **73**, 333–342 (1990).
15. J. Moser, *Nachr. Acad. Wiss. Göttingen II. Math. Phys. Kl.*, 1, 1962.
16. G. J. D. Petrie, submitted to *Astroph. J. Suppl.* (2006)
17. E. Priest and T. Forbes, *Magnetic Reconnection, MHD theory and applications*, Cambridge University Press, Cambridge UK, (2000).
18. T. W. Speiser, *J. Geophys. Res.*, **70** 4129–4226, (1965).
19. N. Vilmer and A. L. MacKinnon in *Energy conversion and particle acceleration in the Solar Coronna* Ed. L. Klein, Lecture Notes in Physics, **612**, 127–160, (2003).